

## Stability of ionic liquid modeled by composite Coulomb-Yukawa potentials

Guilherme Volpe Bossa<sup>1</sup> and Sylvio May<sup>2</sup><sup>1</sup>*Department of Physics, São Paulo State University (UNESP), Institute of Biosciences, Humanities and Exact Sciences, São José do Rio Preto, SP 15054-000, Brazil*<sup>2</sup>*Department of Physics, North Dakota State University, Fargo, North Dakota 58108-6050, USA*

(Received 20 June 2020; accepted 2 August 2020; published 18 August 2020)

An ionic liquid modeled as a densely packed lattice with composite ion-specific Coulomb-Yukawa pair interactions tends to be unstable near a planar electrode, given the Yukawa potential mediates an effective short-range attraction of the ions. We present a comprehensive mean-field model, accounting for ion-specific electrode-ion interactions and for the propagation of the Yukawa field into the electrode. The surface instability precedes the spinodal instability of the ionic liquid and may thus lead to hysteresis and to a large differential capacitance in the metastable region of the phase diagram, but not necessarily to oscillations of the net charge density.

DOI: [10.1103/PhysRevResearch.2.032040](https://doi.org/10.1103/PhysRevResearch.2.032040)

When used as electrolytic capacitors and supercapacitors, ionic liquids utilize properties of the electric double layer (EDL) [1–3]. While EDLs formed in dilute electrolytes are well understood, their counterparts at high ion concentrations or in the absence of solvent are dominated by ion-ion correlations, which are notoriously difficult to model [4–7]. An exception is the solvable model of a lattice Coulomb gas in one dimension, which offers insights into the role of correlations and the emergence of phase transitions between ordered and disordered states [8,9]. Other systematic modeling efforts employ computer simulations [10] or use density functional theory [11–13]. There is also a class of models that attempt to incorporate ion-ion correlations and still preserve the conceptual simplicity of mean-field approaches [14–21]. A premier example for the latter is the incorporation of a nonlocal dielectric constant by Bazant, Storey, and Kornyshev (BSK) [22] into the lattice-based [23] mean-field model of the EDL. Indeed, the BSK model maps to a lattice-based mean-field model for a specific composite Coulomb-Yukawa potential, where the Yukawa potential adds a short-ranged attraction to the long-ranged Coulomb interactions [24]. The competition between short-ranged attraction and long-ranged repulsion may render an ionic liquid unstable in the vicinity of an electrode, with a diverging differential capacitance marking the onset of a phase transition. Limmer [25] has implemented the short-ranged attraction by a phenomenological Landau-Ginzburg approach and Downing *et al.* [26] through a Bragg-Williams free energy. Chao and Wang [27] generalize the BSK model and show that it too predicts a phase transition near an electrode. However, like BSK, they

neglect the penetration of the Yukawa field into the electrode, leading to an incomplete boundary condition. Here, we present a comprehensive lattice-based mean-field model for an ion-specific composite Coulomb-Yukawa pair potential and analyze its structural and thermodynamic predictions. Our mean-field description involves two fields but remains simple enough to afford analytic predictions of all relevant thermodynamic properties. It is also complete in the sense that it allows for arbitrary Yukawa interactions between anion-anion, anion-cation, and cation-cation pairs as well as between ions and the electrode.

Consider a solvent-free ionic liquid that consists of monovalent anions and cations of comparable size with a composite Coulomb-Yukawa interaction potential as function of ion-ion distance  $r$ :  $u_{aa}/k_B T = l_B/r + ae^{-\kappa r}/r$  for an anion-anion pair,  $u_{ac}/k_B T = -l_B/r + be^{-\kappa r}/r$  for an anion-cation pair, and  $u_{cc}/k_B T = l_B/r + ce^{-\kappa r}/r$  for a cation-cation pair, where  $k_B T$  denotes the thermal energy unit (Boltzmann constant times absolute temperature) and  $l_B$  the Bjerrum length. The three interaction strengths of the Yukawa potential contributions,  $a, b, c$ , introduce ion specificity and, as has been suggested previously [22,27–31], account for steric effects and/or ion-ion correlations. We express them conveniently by the matrix  $\mathcal{A}_h = \{\{a, b\}, \{b, c\}\}$ . The real-valued constant  $\kappa$  denotes the inverse decay length of the Yukawa potential. We employ a lattice model [23,32] where every lattice site is occupied by exactly one ion (a cation or an anion) and where we identify the volume  $v$  of a lattice site with the volume of a single ion, the same for anions and cations. We also define the inverse length  $\lambda$  through  $\lambda^2 = 4\pi l_B/v$ .

Coulomb and Yukawa interactions can be described by associated potentials, a scaled Coulomb potential  $\Psi_e$  and two Yukawa potentials,  $\Psi_a$  for anions and  $\Psi_c$  for cations. Two distinct Yukawa potentials are needed in the general case where the lattice is allowed to also be populated by void sites and where  $\mathcal{A}_h$  is not singular [31]. For an ionic liquid with a single planar electrode immersed at position  $x = 0$  and the  $x$

axis pointing normal into the bulk, the three potentials  $\Psi_e(x)$ ,  $\Psi_a(x)$ , and  $\Psi_c(x)$  satisfy three nonlinear differential equations [33]

$$\begin{aligned} \frac{1}{\lambda^2} \Psi_e'' &= \frac{\phi_0}{q} (e^{\Psi_e - \Psi_a} - e^{-\Psi_e - \Psi_c}), \\ \left( \Psi_a'' - \kappa^2 \Psi_a \right) &= -\frac{4\pi}{v} \frac{\phi_0}{q} \mathcal{A}_h \left( e^{\Psi_e - \Psi_a} - q \right), \\ \left( \Psi_c'' - \kappa^2 \Psi_c \right) &= -\frac{4\pi}{v} \frac{\phi_0}{q} \mathcal{A}_h \left( e^{-\Psi_e - \Psi_c} - q \right). \end{aligned} \quad (1)$$

Here,  $\phi_0$  is the bulk volume fraction of cations and anions,  $q = 1 + \phi_0(e^{\Psi_e - \Psi_a} + e^{-\Psi_e - \Psi_c} - 2)$  is a partition sum, and a prime denotes a derivative with respect to  $x$ . Equations (1) are valid at the mean-field level and must be solved with respect to the boundary conditions [33]

$$\begin{aligned} \Psi_e'(0) &= -\lambda^2 v \frac{\sigma_e}{e}, \\ \left( \Psi_a'(0) - \kappa \Psi_a(0) \right) &= -4\pi \mathcal{A}_h \left( \frac{\sigma_a}{\sigma_c} \right), \\ \left( \Psi_c'(0) - \kappa \Psi_c(0) \right) &= -4\pi \mathcal{A}_h \left( \frac{\sigma_c}{\sigma_a} \right), \end{aligned} \quad (2)$$

where  $\sigma_e$  is the electrostatic surface charge density of the electrode and  $e$  the elementary charge. Furthermore,  $\sigma_a$  and  $\sigma_c$  denote the surface densities of sources for the Yukawa potential, which describe preferential, ion-specific interactions of the ions with the electrode. All three potentials vanish in the bulk, at  $x \rightarrow \infty$ .

A densely packed ionic liquid has all lattice sites occupied by ions; this corresponds to  $\phi_0 = 1/2$ . In this case, which is our focus, the equations for the two Yukawa potentials in Eqs. (1) are no longer independent, suggesting to define a single new potential  $\Psi_h = (\Psi_c - \Psi_a)/2$ . Equations (1) then become

$$\begin{aligned} \frac{1}{\lambda^2} \Psi_e'' &= \tanh(\Psi_e + \Psi_h), \\ \Psi_h'' - \kappa^2 \Psi_h &= -\alpha^2 \tanh(\Psi_e + \Psi_h), \end{aligned} \quad (3)$$

with the Yukawa interaction strength  $\alpha$ , defined through  $\alpha^2 = (2b - a - c)\pi/v$ . Note that  $\alpha$  is real valued if the Yukawa interactions mediate an effective attraction,  $2b > a + c$ . The boundary conditions, Eqs. (2), read

$$\Psi_e'(0) = -\lambda s_e, \quad \Psi_h'(0) - \kappa \Psi_h(0) = -\kappa s_h, \quad (4)$$

where we have defined the scaled surface charge density  $s_e = \lambda v \sigma_e / e$  and the corresponding scaled surface source density for the Yukawa potential  $s_h = 2\pi[\sigma_c(c - b) - \sigma_a(a - b)]/\kappa$ . Equations (3) and (4) also follow from minimizing the free energy  $F$  per unit area  $A$  of the electrode,

$$\begin{aligned} \frac{F}{Ak_B T} &= \frac{1}{v} \int_{-\infty}^{\infty} dx \left[ -\frac{1}{2\lambda^2} \Psi_e'^2 + \frac{1}{2\alpha^2} (\Psi_h'^2 + \kappa^2 \Psi_h^2) \right] \\ &+ \frac{1}{v} \int_0^{\infty} dx [\phi_a \ln \phi_a + \phi_c \ln \phi_c] \\ &+ \frac{1}{v} \int_0^{\infty} dx \left\{ \Psi_e \left[ \phi_c - \phi_a + \delta(0) \frac{s_e}{\lambda} \right] \right\} \\ &+ \frac{1}{v} \int_0^{\infty} dx \left\{ \Psi_h \left[ \phi_c - \phi_a + \delta(0) \frac{\kappa}{\lambda^2} s_h \right] \right\} \end{aligned} \quad (5)$$

with respect to  $\Psi_e$ ,  $\Psi_h$ ,  $\phi_c$ , and  $\phi_a$ . The local volume fractions  $\phi_c$  and  $\phi_a$  of the cations and anions, respectively, satisfy

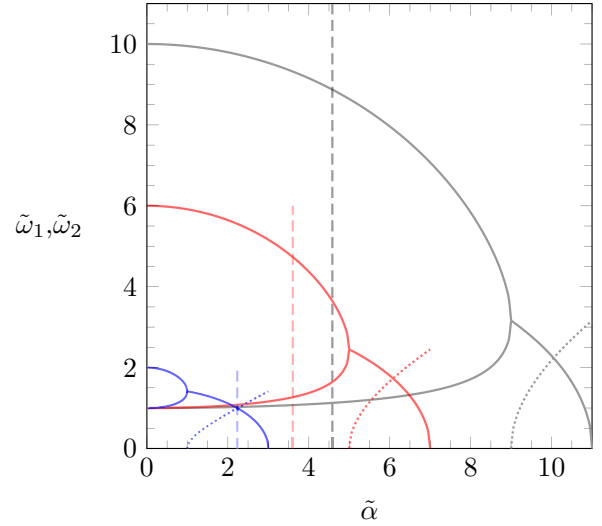


FIG. 1. The real-valued  $\tilde{\omega}_1$  and  $\tilde{\omega}_2$  (left branch, for  $\tilde{\alpha} < \tilde{\lambda} - 1$ ), and the real and imaginary parts of  $\tilde{\omega}_1 = \tilde{\omega}_r + i\tilde{\omega}_c$  and  $\tilde{\omega}_2 = \tilde{\omega}_r - i\tilde{\omega}_c$  (right branch, for  $\tilde{\lambda} - 1 < \tilde{\alpha} < \tilde{\lambda} + 1$ ) as a function of  $\tilde{\alpha}$  for fixed  $\tilde{\lambda} = 2$  (blue),  $\tilde{\lambda} = 6$  (red), and  $\tilde{\lambda} = 10$  (gray). The real part  $\tilde{\omega}_r$  is shown by solid lines and the imaginary part  $\tilde{\omega}_c$  by dotted lines. At the branching point  $\tilde{\omega}_1 = \tilde{\omega}_2 = \tilde{\omega}_r$  and  $\tilde{\omega}_c = 0$ . The color-matching vertical dashed lines mark the point  $\tilde{\alpha} = \sqrt{1 + 2\tilde{\lambda}}$  where the differential capacitance diverges.

$\phi_c + \phi_a = 1$  in a densely filled lattice. The integral in the first line of Eq. (5) extends over all space to account for the necessary existence of the fields inside the electrode, for  $x < 0$ . In that region, the Coulomb field remains constant whereas the Yukawa field decays exponentially. The integral in the second line describes the ion mixing entropy. The last two integrals account for interactions of the Coulomb and Yukawa potentials with the ions (for  $x > 0$ ) and with the sources on the electrode surface (at  $x = 0$ ).

The limit of small potentials allows us to linearize Eqs. (3) and reexpress them in terms of a fourth-order equation for the (scaled) Coulomb potential,

$$\Psi_e'''' - (\kappa^2 + \lambda^2 - \alpha^2) \Psi_e'' + \kappa^2 \lambda^2 \Psi_e = 0. \quad (6)$$

Its solution  $\Psi_e(x) = A_1 e^{-\omega_1 x} + A_2 e^{-\omega_2 x}$ , which adopts the bulk value  $\Psi_e(x \rightarrow \infty) = 0$ , is associated with the two inverse characteristic lengths  $\omega_1$  and  $\omega_2$  that satisfy the algebraic relations

$$\omega_1^2 + \omega_2^2 = \kappa^2 + \lambda^2 - \alpha^2, \quad \omega_1^2 \omega_2^2 = \kappa^2 \lambda^2. \quad (7)$$

It is useful to introduce scaled quantities,  $\tilde{\lambda} = \lambda/\kappa$ ,  $\tilde{\alpha} = \alpha/\kappa$ ,  $\tilde{\omega}_1 = \omega_1/\kappa$ , and  $\tilde{\omega}_2 = \omega_2/\kappa$ . The latter two,  $\tilde{\omega}_1 = \tilde{\omega}_1(\tilde{\lambda}, \tilde{\alpha})$  and  $\tilde{\omega}_2 = \tilde{\omega}_2(\tilde{\lambda}, \tilde{\alpha})$ , are fully determined by  $\tilde{\lambda}$  and  $\tilde{\alpha}$  according to Eq. (7). Figure 1 shows how  $\tilde{\omega}_1$  and  $\tilde{\omega}_2$  depend on  $\tilde{\alpha}$  for fixed  $\tilde{\lambda} = 2$  (blue),  $\tilde{\lambda} = 6$  (red), and  $\tilde{\lambda} = 10$  (gray).

We find for the electrostatic surface potential  $\Psi_0 = \Psi_e(0) = A_1 + A_2$  the explicit expression

$$\Psi_0 = (\tilde{\omega}_1 + \tilde{\omega}_2 - \tilde{\lambda}) s_e - \frac{\tilde{\lambda}}{\tilde{\omega}_1 + \tilde{\omega}_2 + \tilde{\lambda} + 1} s_h, \quad (8)$$

where

$$\tilde{\omega}_1 + \tilde{\omega}_2 = \sqrt{(1 + \tilde{\lambda})^2 - \tilde{\alpha}^2} \quad (9)$$

is real and positive as long as the bulk of the ionic liquid is structurally stable (for  $\tilde{\alpha} < 1 + \tilde{\lambda}$ ).

The differential capacitance  $C_{\text{diff}} = d\sigma_e/d\Phi_0$  is the derivative of the surface charge density  $\sigma_e$  with respect to the electrostatic surface potential  $\Phi_0 = \Psi_0 \times k_B T/e$ . We define a scaled (dimensionless) differential capacitance and calculate it from Eq. (8):

$$\bar{C}_{\text{diff}} = \frac{C_{\text{diff}}}{\lambda \epsilon \epsilon_0} = \frac{1}{\left(\frac{d\Psi_0}{ds_e}\right)} = \frac{1}{\sqrt{(1 + \tilde{\lambda})^2 - \tilde{\alpha}^2} - \tilde{\lambda}}. \quad (10)$$

Stability of the ionic liquid at the electrode requires  $\bar{C}_{\text{diff}} > 0$ . It can immediately be observed that  $\bar{C}_{\text{diff}}$  diverges if

$$\tilde{\alpha} = \sqrt{1 + 2\tilde{\lambda}}, \quad (11)$$

which is displayed in Fig. 1 as vertical dashed lines, corresponding to the three values  $\tilde{\lambda} = 2$  (blue),  $\tilde{\lambda} = 6$  (red), and  $\tilde{\lambda} = 10$  (gray). Any choice of  $\tilde{\alpha}$  with  $0 < \tilde{\alpha} < 1 + \tilde{\lambda}$  will give rise to a positive real  $\tilde{\lambda}$  at which  $\bar{C}_{\text{diff}}$  diverges. We discuss special cases encountered for growing  $\alpha$ :

(1)  $\tilde{\alpha} = 0$  leads to  $\tilde{\omega}_1 = 1$ ,  $\tilde{\omega}_2 = \tilde{\lambda}$ , and  $\bar{C}_{\text{diff}} = 1$ , thus recovering the classical lattice-based Poisson-Boltzmann result [32] in the absence of Yukawa interactions.

(2)  $\tilde{\alpha} = \tilde{\lambda} - 1$  implies  $\tilde{\omega}_1 = \tilde{\omega}_2 = \sqrt{\tilde{\lambda}}$  to transition from being both real valued to being complex conjugate numbers. Double-exponential decay is thus replaced by damped oscillations of the electrostatic potential  $\Psi_e(x)$ . For  $\tilde{\lambda} < 4$  we obtain  $\bar{C}_{\text{diff}} = 1/(2\sqrt{\tilde{\lambda}} - \tilde{\lambda})$ .

(3)  $\tilde{\alpha} = \tilde{\lambda}$  reproduces the BSK model [22]  $l_B = -a = -c = b$  and thus models the specific interaction potential  $u_{aa} = u_{cc} = -u_{ac} = k_B T l_B (1 - e^{-\kappa r})/r$ . For  $\tilde{\lambda} < 1 + \sqrt{2}$  we obtain  $\bar{C}_{\text{diff}} = 1/(\sqrt{1 + 2\tilde{\lambda}} - \tilde{\lambda})$ .

(4)  $\tilde{\alpha} = \sqrt{\tilde{\lambda}^2 + 1}$  implies the complex conjugates  $\tilde{\omega}_{1/2} = \sqrt{\tilde{\lambda}/2} (1 \pm i)$  to have the same magnitudes of their real and imaginary parts. For  $\tilde{\lambda} < 2$  this leads to  $\bar{C}_{\text{diff}} = 1/(\sqrt{2\tilde{\lambda}} - \tilde{\lambda})$ .

(5)  $\tilde{\alpha} = \tilde{\lambda} + 1$  marks the spinodal boundary, where  $\tilde{\omega}_1 = i\tilde{\lambda}$  and  $\tilde{\omega}_2 = -i\tilde{\lambda}$  transition from complex conjugate to imaginary numbers, indicating the onset of oscillations and thus a structural instability of the ionic liquid in its bulk.

Stability of the ionic liquid in the bulk demands  $\tilde{\alpha} < \tilde{\lambda} + 1$ . Yet, already for  $\tilde{\alpha} = \sqrt{1 + 2\tilde{\lambda}}$  the differential capacitance diverges, which marks the onset of an instability at the surface of the electrode. The surface instability always precedes the bulk instability. Following phase separation, for  $\tilde{\alpha} > \sqrt{1 + 2\tilde{\lambda}}$ , the ionic liquid will always exhibit damped oscillations of its local net charge density if  $\tilde{\lambda} < 4$ . For  $\tilde{\lambda} > 4$ , there is a range  $\sqrt{1 + 2\tilde{\lambda}} < \tilde{\alpha} < \tilde{\lambda} - 1$ , where the electrode triggers a phase transition, yet without oscillations of the local net charge density.

For the BSK model [22],  $\tilde{\alpha} = \tilde{\lambda}$  (corresponding to  $-a = -c = b = l_B$ ), the differential capacitance diverges for  $\tilde{\lambda} = \lambda/\kappa = 1 + \sqrt{2}$ . Recalling the definition  $\lambda^2 = 4\pi l_B/\nu$  and using the values  $\kappa = 1 \text{ nm}^{-1}$  and  $\nu \approx 1 \text{ nm}^3$  (which are both determined by the ion size), we find that  $l_B = \nu(1 + \sqrt{2})^2 \kappa^2 / (4\pi) = 0.46 \text{ nm}$  would already lead to a diverging

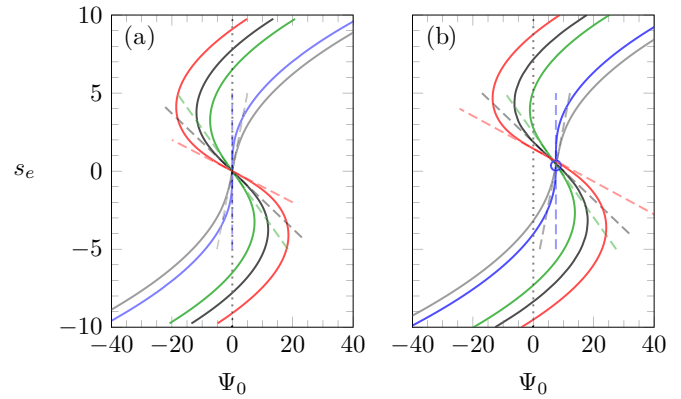


FIG. 2. Scaled surface charge density  $s_e = \lambda \nu \sigma_e / e$  as a function of the electrostatic surface potential  $\Psi_0$  for  $\tilde{\alpha} = 0$  (gray),  $\tilde{\alpha} = \sqrt{21}$  (blue),  $\tilde{\alpha} = 9$  (green),  $\tilde{\alpha} = \sqrt{101}$  (black), and  $\tilde{\alpha} = 11$  (red). Solid lines represent solutions of the nonlinear model according to Eqs. (3) and (4). Broken lines mark the slopes at the points of inflection. The blue open circle (b) is located at position  $\{\Psi_0, s_e\}$  according to Eq. (12). All curves are calculated for  $\lambda = 10/\text{nm}$  and  $\kappa = 1/\text{nm}$ , as well as  $s_h = 0$  (a) and  $s_h = -2\pi \times 2.5$  (b).

$\bar{C}_{\text{diff}}$ . Because this is even smaller than the Bjerrum length in water, we conclude that the choice  $-a = -c = b = l_B$  leads to the prediction of a generic surface instability of ionic liquids.

If we do not assume  $-a = -c = b = l_B$  but instead fix the Bjerrum length  $l_B \approx 8 \text{ nm}$  as well as  $\kappa = 1 \text{ nm}^{-1}$  and  $\nu \approx 1 \text{ nm}^3$ , then we find  $\lambda = \sqrt{4\pi l_B/\nu} = 10 \text{ nm}^{-1}$  and thus  $\tilde{\lambda} = 10$ . The gray curves in Fig. 1 correspond to that case. Bulk and surface instability at the electrode occur at  $\tilde{\alpha} = \tilde{\lambda} + 1 = 11$  and  $\tilde{\alpha} = \sqrt{1 + 2\tilde{\lambda}} = \sqrt{21} \approx 4.6$ , respectively. The latter is marked by the gray vertical dashed line in Fig. 1.

In Figs. 2 and 3 we expand our analytic results for the linearized model by a numerical analysis of the nonlinear model, as characterized by Eqs. (3) and (4). As in the preceding paragraph, we are using the generic choices  $\lambda = 10/\text{nm}$  and  $\kappa = 1/\text{nm}$ , and for  $\alpha$  we scan through a set of relevant values:

gray curves:  $\tilde{\alpha} = 0$ ;

blue curves:  $\tilde{\alpha} = \sqrt{1 + 2\tilde{\lambda}} = \sqrt{21} \approx 4.58$ ; here  $\bar{C}_{\text{diff}}$  diverges;

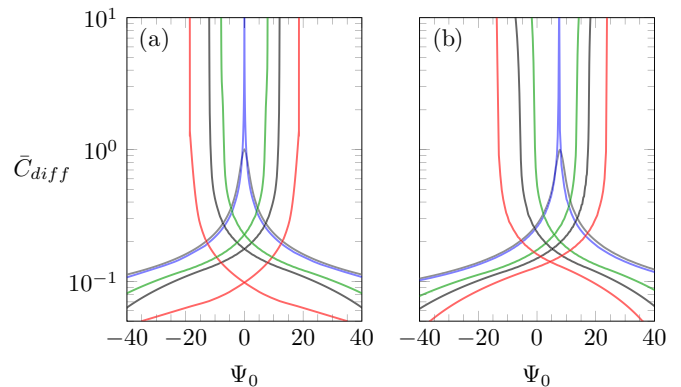


FIG. 3.  $\bar{C}_{\text{diff}}$  as a function of  $\Psi_0$  for  $\tilde{\alpha} = 0$  (gray),  $\tilde{\alpha} = \sqrt{21}$  (blue),  $\tilde{\alpha} = 9$  (green),  $\tilde{\alpha} = \sqrt{101}$  (black), and  $\tilde{\alpha} = 11$  (red). All curves are calculated for  $\lambda = 10/\text{nm}$  and  $\kappa = 1/\text{nm}$ , as well as  $s_h = 0$  (a) and  $s_h = -2\pi \times 2.5$  (b).

green curves:  $\tilde{\alpha} = \tilde{\lambda} - 1 = 9$ , corresponding to case (2) above;

black curves:  $\tilde{\alpha} = \sqrt{\tilde{\lambda}^2 + 1} = \sqrt{101} \approx 10.05$ , corresponding to case (4) above;

red curves:  $\tilde{\alpha} = \tilde{\lambda} + 1 = 11$ , corresponding to case (5) above.

Figure 2 shows the relation between scaled surface charge density  $s_e$  and surface potential  $\Psi_0$  for  $s_h = 0$  (a) and  $s_h = -2\pi \times 2.5$  (b). The condition  $\sigma_c(c - b) = \sigma_a(a - b)$  implies  $s_h = 0$  [Fig. 2(a)], which renders the linearized model valid in the vicinity of the point  $\Psi_0 = s_e = 0$ . Indeed, the slopes (dashed lines) of the calculated curves (solid lines) at  $\Psi_0 = s_e = 0$  correspond exactly to  $\tilde{C}_{\text{diff}} = ds_e/d\Psi_0$  according to Eq. (8). The slope is positive for  $\tilde{\alpha} = 0$  (gray line), increases to infinity at  $\tilde{\alpha} = \sqrt{21}$  (blue line), and then adopts negative values thereafter (green, black, red lines). For  $s_h = -2\pi \times 2.5$  [Fig. 2(b)] there exists, strictly speaking, no point in the vicinity of which the linear model is valid. Curves corresponding to different  $\tilde{\alpha}$  do not intersect at a single point. To a good approximation, however, they do, and we can calculate that point writing Eq. (8) as  $\Psi_0 = f(\tilde{\alpha})s_e + g(\tilde{\alpha})s_h$ . From  $0 = d\Psi_0/d\tilde{\alpha} = f'(\tilde{\alpha})s_e + g'(\tilde{\alpha})s_h$  we deduce  $s_e = -[g'(\tilde{\alpha})/f'(\tilde{\alpha})]s_h$  and  $\Psi_0 = -\{f(\tilde{\alpha})[g'(\tilde{\alpha})/f'(\tilde{\alpha})] + g(\tilde{\alpha})\}s_h$ . This location depends only weakly on  $\tilde{\alpha}$  as long as  $\tilde{\alpha} \lesssim \tilde{\lambda}$ . We may chose  $\tilde{\alpha} = 0$  or, more conveniently, the critical value  $\tilde{\alpha} = \sqrt{1 + 2\tilde{\lambda}}$ , which leads to the simple result

$$s_e = -\frac{\tilde{\lambda}}{(1 + 2\tilde{\lambda})^2}s_h, \quad \Psi_0 = -\frac{\tilde{\lambda}}{1 + 2\tilde{\lambda}}s_h. \quad (12)$$

This point also approximates the point of inflection, where the diverging differential capacitance marks the onset of the phase transition near the electrode. The blue open circle in diagram (b) of Fig. 2 indicates the location defined in Eq. (12).

Figure 3 shows the scaled differential capacitance  $\tilde{C}_{\text{diff}} = ds_e/d\Psi_0$  calculated from Fig. 2 for  $s_h = 0$  [diagram (a)] and  $s_h = -2\pi \times 2.5$  [diagram (b)]. The gray line, where  $\tilde{\alpha} = 0$ , corresponds to the well-known bell-shaped profile [32] of the lattice model in the presence of only Coulomb interactions,  $\tilde{C}_{\text{diff}} = |\tanh \Psi_0|/\sqrt{2 \ln(\cosh \Psi_0)}$ . The blue line, where  $\tilde{\alpha} = \sqrt{21}$ , marks the onset of the ionic liquid's instability at the electrode surface:  $\tilde{C}_{\text{diff}}$  diverges at  $\Psi_0 = -s_h\tilde{\lambda}/(1 + 2\tilde{\lambda})$ . Spatially oscillating ion densities start developing at the green line (where  $\tilde{\alpha} = 9$ ). The two characteristic lengths of these oscillations become equal at the black line (where  $\tilde{\alpha} = \sqrt{101}$ ). Eventually, at the red line (where  $\tilde{\alpha} = 11$ ), the characteristic length corresponding to the exponential decay grows to infinity, indicating the crossing of the spinodal line beyond which the ionic liquid is locally unstable. Between the blue and red line ( $\sqrt{21} < \tilde{\alpha} < 11$ ), the ionic liquid is subject to a first-order phase transition in the vicinity of the electrode. That is, the surface charge density undergoes a discontinuous jump as a function of the surface potential, which in the thermodynamically stable case leads to the lower branch of  $\tilde{C}_{\text{diff}}$  for the curves marked green, black, and red. If the system transitions into the metastable case,  $\tilde{C}_{\text{diff}}$  grows further.

The BSK model [22] applies to the special case  $\tilde{\alpha} = \tilde{\lambda}$  that represents the specific Coulomb-Yukawa interaction potential

$u_{aa} = u_{cc} = -u_{ac} = k_B T l_B (1 - e^{-\kappa r})/r$ . Based on the single potential  $\Psi = \Psi_e + \Psi_h$  BSK state the modified Poisson equation  $\Psi'' - \Psi'''/\kappa^2 = -\lambda^2(\phi_c - \phi_a)$  and electrostatic energy  $U$  per unit area  $A$  of the electrode,

$$\frac{U}{Ak_B T} = \frac{1}{2\lambda^2 v} \int dx \left( \Psi'^2 + \frac{1}{\kappa^2} \Psi''^2 \right). \quad (13)$$

The corresponding equations of our present approach [see Eq. (5)] are  $-\Psi_e''/\lambda^2 = \phi_c - \phi_a$  and  $\Psi_h'' - \kappa^2 \Psi_h = \lambda^2(\phi_c - \phi_a)$  as well as

$$\frac{U}{Ak_B T} = \frac{1}{2\lambda^2 v} \int dx [\Psi_e'^2 - (\Psi_h'^2 + \kappa^2 \Psi_h^2)]. \quad (14)$$

It is straightforward to show that both approaches are equivalent. The boundary condition at the electrode surface,  $\Psi'''(0) = 0$ , used in the BSK model [22], has recently been restated [24] to be  $\Psi'''(0) - \kappa \Psi''(0) = 0$ , which enforces continuity of the Maxwell stress at the charged electrode. Our present approach produces the more general boundary condition

$$\Psi'''(0) - \kappa \Psi''(0) = \lambda^2 \kappa^2 v (\sigma_c - \sigma_a), \quad (15)$$

which follows upon noting  $s_h = -\lambda^2 v (\sigma_c - \sigma_a)/\kappa$  and inserting  $\Psi_h = \Psi''/\kappa^2$  into Eq. (4). The additional term  $\sim(\sigma_c - \sigma_a)$  appears in the presence of asymmetric Yukawa interactions of the cations and anions with the electrode ( $\sigma_c \neq \sigma_a$ ).

Chao and Wang [27] employ two potentials, Coulomb and Yukawa, to model the composite pair interaction  $u_{aa} = u_{cc} = -u_{ac} = k_B T l_B (1 - w e^{-\kappa r})/r$ , where  $w$  is a dimensionless parameter. This generalizes the BSK model to capture the more general case  $a = c = -b = w l_B$  and thus  $\alpha = \sqrt{w} \lambda$ . Chao and Wang obtain the same spinodal as we do in our work. However, their boundary condition for the Yukawa potential,  $\Psi_h'(0) = 0$  [instead of Eq. (4)], is the same as that used in the BSK model [22]; it does not employ  $\sigma_e$  and  $\sigma_c$  and, more importantly, ignores the penetration of the Yukawa potential into the electrode. This overestimates the instability of the ionic liquid at the electrode surface [leading to a diverging  $\tilde{C}_{\text{diff}}$  already for  $\tilde{\alpha} = \sqrt{1 + \tilde{\lambda}}$  instead of  $\tilde{\alpha} = \sqrt{1 + 2\tilde{\lambda}}$  according to Eq. (11)]. Despite these differences, the ability of the model from Chao and Wang [27] to account for experimentally observed hysteresis effects [34,35] applies analogously to our present model.

In summary, we present a comprehensive mean-field description of an ionic liquid with ion-specific, composite Coulomb and Yukawa interactions on a densely packed lattice. The additional Yukawa contribution serves as a representation of ion-ion correlations and/or of ion-specific short-range non-electrostatic ion-ion interactions. Our model generalizes the BSK model [22] and provides a straightforward derivation of the boundary conditions on the electrode. The linearized limit affords simple analytic results for all structural and thermodynamic properties, including the differential capacitance which diverges at the onset of the ionic liquid's instability near an inserted electrode.

G.V.B. acknowledges a postdoctoral fellowship from the São Paulo Research Foundation (FAPESP, Grant No. 2017/21772-2). S.M. thanks ND EPSCoR for support.



- [1] T. Sato, G. Masuda, and K. Takagi, *Electrochim. Acta* **49**, 3603 (2004).
- [2] M. A. Gebbie, A. M. Smith, H. A. Dobbs, G. G. Warr, X. Banquy, M. Valtiner, M. W. Rutland, J. N. Israelachvili, S. Perkin, R. Atkin *et al.*, *Chem. Commun.* **53**, 1214 (2017).
- [3] A. Eftekhari, *Energy Storage Mater.* **9**, 47 (2017).
- [4] R. R. Netz and H. Orland, *Eur. Phys. J. E* **1**, 203 (2000).
- [5] Y. Levin, *Rep. Prog. Phys.* **65**, 1577 (2002).
- [6] C. D. Santangelo, *Phys. Rev. E* **73**, 041512 (2006).
- [7] A. Naji, M. Kanduč, J. Forsman, and R. Podgornik, *J. Chem. Phys.* **139**, 150901 (2013).
- [8] V. Démery, D. S. Dean, T. C. Hammant, R. R. Horgan, and R. Podgornik, *Europhys. Lett.* **97**, 28004 (2012).
- [9] V. Démery, R. Monsarrat, D. S. Dean, and R. Podgornik, *Europhys. Lett.* **113**, 18008 (2016).
- [10] E. J. Maginn, *J. Phys.: Condens. Matter* **21**, 373101 (2009).
- [11] D.-e. Jiang, D. Meng, and J. Wu, *Chem. Phys. Lett.* **504**, 153 (2011).
- [12] J. Wu, T. Jiang, D.-e. Jiang, Z. Jin, and D. Henderson, *Soft Matter* **7**, 11222 (2011).
- [13] S. Lamperski, M. Kaja, L. B. Bhuiyan, J. Wu, and D. Henderson, *J. Chem. Phys.* **139**, 054703 (2013).
- [14] Y. Han, S. Huang, and T. Yan, *J. Phys.: Condens. Matter* **26**, 284103 (2014).
- [15] R. Blossey, A. C. Maggs, and R. Podgornik, *Phys. Rev. E* **95**, 060602(R) (2017).
- [16] A. A. Lee, C. S. Perez-Martinez, A. M. Smith, and S. Perkin, *Phys. Rev. Lett.* **119**, 026002 (2017).
- [17] N. Gavish, D. Elad, and A. Yochelis, *J. Phys. Chem. Lett.* **9**, 36 (2018).
- [18] N. B. Ludwig, K. Dasbiswas, D. V. Talapin, and S. Vaikuntanathan, *J. Chem. Phys.* **149**, 164505 (2018).
- [19] R. M. Adar, S. A. Safran, H. Diamant, and D. Andelman, *Phys. Rev. E* **100**, 042615 (2019).
- [20] Y. Avni, R. M. Adar, and D. Andelman, *Phys. Rev. E* **101**, 010601(R) (2020).
- [21] J. P. de Souza, Z. A. Goodwin, M. McEldrew, A. A. Kornyshev, and M. Z. Bazant, *arXiv:2005.04270* [Phys. Rev. Lett. (to be published)].
- [22] M. Z. Bazant, B. D. Storey, and A. A. Kornyshev, *Phys. Rev. Lett.* **106**, 046102 (2011).
- [23] I. Borukhov, D. Andelman, and H. Orland, *Phys. Rev. Lett.* **79**, 435 (1997).
- [24] J. P. de Souza and M. Z. Bazant, *J. Phys. Chem. C* **124**, 11414 (2020).
- [25] D. T. Limmer, *Phys. Rev. Lett.* **115**, 256102 (2015).
- [26] R. Downing, B. K. Berntson, G. V. Bossa, and S. May, *J. Chem. Phys.* **149**, 204703 (2018).
- [27] H. Chao and Z.-G. Wang, *J. Phys. Chem. Lett.* **11**, 1767 (2020).
- [28] R. D. Coalson, A. M. Walsh, A. Duncan, and N. Ben-Tal, *J. Chem. Phys.* **102**, 4584 (1995).
- [29] F. Paillusson and R. Blossey, *Phys. Rev. E* **82**, 052501 (2010).
- [30] S. Buyukdagli and T. Ala-Nissila, *J. Chem. Phys.* **136**, 074901 (2012).
- [31] D. L. Caetano, G. V. Bossa, V. M. de Oliveira, M. A. Brown, S. J. de Carvalho, and S. May, *Phys. Chem. Chem. Phys.* **18**, 27796 (2016).
- [32] A. A. Kornyshev, *J. Phys. Chem. B* **111**, 5545 (2007).
- [33] J. Spaight, R. Downing, S. May, S. J. de Carvalho, and G. V. Bossa, *Phys. Rev. E* **101**, 052603 (2020).
- [34] T. R. Gore, T. Bond, W. Zhang, R. W. Scott, and I. J. Burgess, *Electrochem. Commun.* **12**, 1340 (2010).
- [35] M. Drüschler, B. Huber, S. Passerini, and B. Roling, *J. Phys. Chem. C* **114**, 3614 (2010).